ChemPhotoChem
Research Article
doi.org/10.1002/cptc.202300343
Chemistry Europe
European Chemical Societies Publishing
www.chemphotochem.org

Enhanced Intersystem Crossing in a Thiohelicene

Sebastian Bergwinkl,[a] Patrick Nuernberger,[a] Bernhard Dick,*[a] and Roger Jan Kutta*[a]

The photophysics of a helicene derivative in which two benzene units are replaced by thiophene units (thiohelicene, **6H**) was studied by steady state and transient absorption and emission spectroscopies covering time ranges from femtoseconds to minutes. Efficient intersystem crossing (ISC) to the triplet state was observed, by far exceeding that of the parent helicene and the corresponding oxo-helicene. Quantum chemical calculations indicate that the helical distortion and the heavy atom effect of sulfur cooperate in promoting spin-orbit coupling, and that the most efficient decay channel involved the T_2 or even the T_3 state. These insights can help in the design of more efficient triplet sensitizers for many applications.

Introduction

Organic molecules with long-lived triplet states are used for many applications. For instance, they can serve as sensitizers in photochemical reactions and photocatalysis,[1,2] as singlet oxygen generators for photodynamic cancer therapy,[3–5] or in technical devices like photovoltaics.[6,7] Important properties for these applications are an efficient formation of the triplet state after electronic excitation and a long triplet lifetime. Hence, intersystem crossing (ISC) from the excited singlet state (S_1) to the triplet state(s) (T_n) should be fast with high yield, but ISC from T_1 to the ground state (S_0) should be slow. The key property for ISC is the spin-orbit coupling (SOC) between the respective singlet and triplet states. The corresponding matrix element (SOCME) vanishes when singlet and triplet have the same orbital occupation. They are usually small when both states have $\pi\pi^*$ character in a planar molecule (El-Sayed rule[8,9]). This has led to the proposal that twisting of a molecular π-electron system might enhance ISC,[10] which was also confirmed both theoretically and experimentally for various systems,[11–21] among them carbon nanotubes which exhibit an especially strong intramolecular curvature.[22–24] However, whereas in some cases a strong increase in the efficiency of ISC by twisting has been observed, other twisted molecules showed just the opposite effect, and it was pointed out that other factors also play an important role.[25–28]

Such a well-known factor is the effect of so-called heavy atoms,[29,30] *i.e.*, atoms with a large nuclear charge. As the velocities of the inner electrons approach a substantial fraction of the velocity of light, relativistic effects and, thus, SOC becomes large. Indeed, ISC in organic chromophores can be enhanced by substituents like bromine or iodine. The effect is even larger in metal organic compounds when atomic orbitals of the metal contribute to the molecular orbitals involved in the electronic excitations of interest. However, typical metal atoms used in this context like Ru, Ir, or Pt are expensive and frequently too poisonous for medical applications. The carbon iodine bond (C–I) is usually photolabile, *vide infra*. Most of all, however, the heavy atom effect also increases the rate of ISC from T_1 to S_0, shortening the lifetime of the T_1 state and reducing its availability for the desired reactions.

Among the numerous molecular classes which allow for a significant and persisting twisting of the molecular π-system, helicene systems with their intrinsic helicoidal structure are especially attractive. Research on helicenes has evolved tremendously over the last century with applications in catalysis, biochemistry, organic photovoltaics, optoelectronic devices, and beyond.[31–34] Many issues yet remain unsolved, e.g., the role of SOC and vibronic coupling after photoexcitation, which are addressed in topical studies with advanced ultrafast spectroscopic[35–39] and theoretical[40–42] approaches. Especially for utilization in optoelectronics, further criteria for an appropriate material comprise the conducting properties, the insensitivity to the environment, and the robustness, e.g., with regard to many photoexcitations.

In this regard, new helicene-like materials are perpetually conceived and synthesized, as for instance thiohelicenes based on dibenzothiophene units.[43,44] In this paper, the photophysical properties of two such thiohelicenes derivatives (Figure 1a) have been studied by several steady-state and time-resolved optical spectroscopic methods with an emphasis on elucidating the ISC processes. The impact of the helicoidal structure as well as the internal heavy-atom effect on the ISC processes has been elaborated together with a supportive theoretical investigation. Furthermore, indications for a light-induced transient ring-closure reaction are presented, and its feasibility is investigated by quantum chemical calculations.

[a] S. Bergwinkl, P. Nuernberger, B. Dick, R. J. Kutta
Institut für Physikalische und Theoretische Chemie, Universität Regensburg,Universitätsstraße 31, 93053 Regensburg, Germany
E-mail: bernhard.dick@ur.de
roger-jan.kutta@ur.de

Supporting information for this article is available on the WWW under https://doi.org/10.1002/cptc.202300343

Research Article
doi.org/10.1002/cptc.202300343

Chemistry Europe
European Chemical Societies Publishing

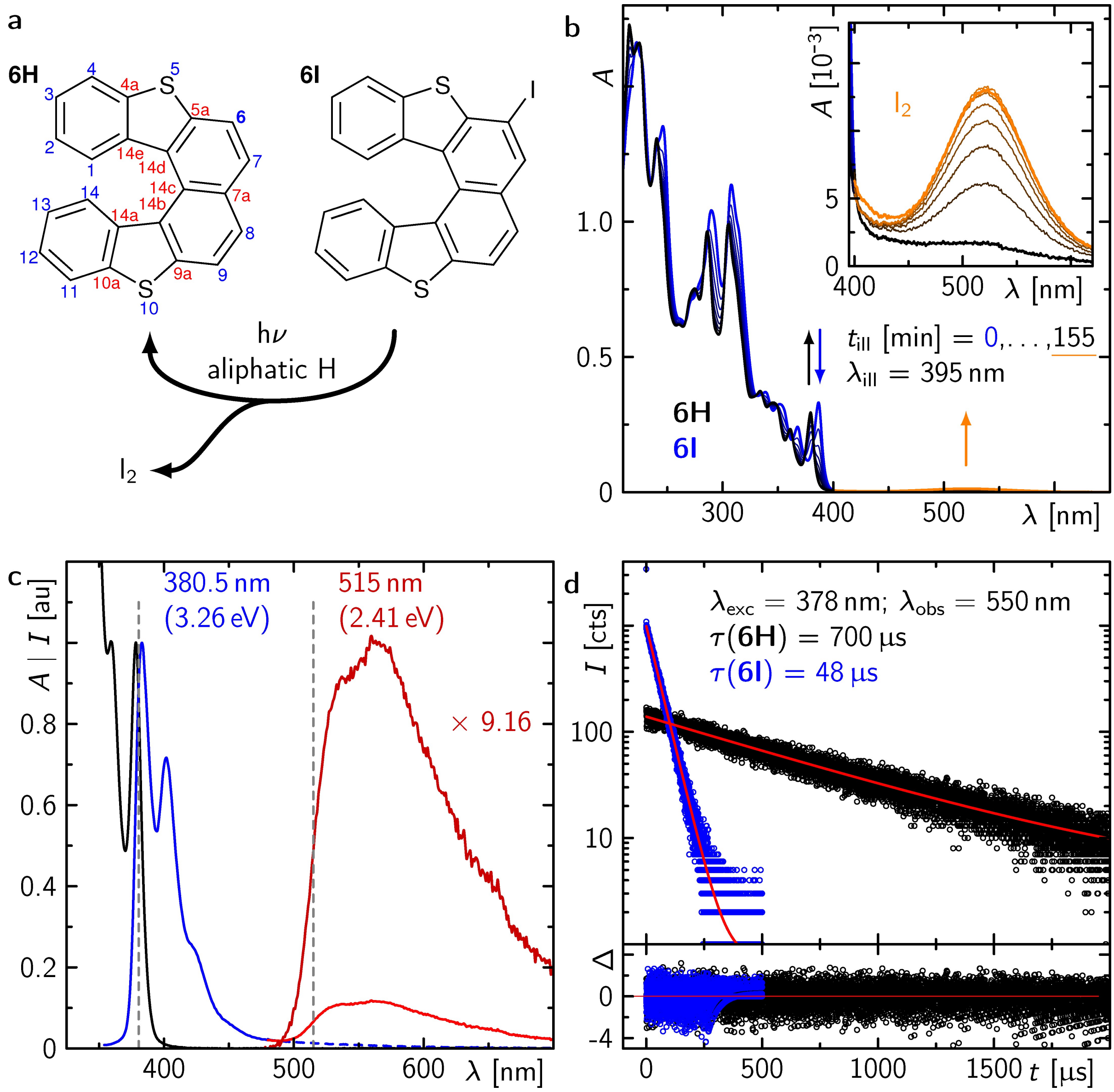

Figure 1. **a**: Chemical structures of compounds **6H** and **6I** and schematic photoconversion of **6I** into **6H**. **b**: Sequence of absorption spectra after stepwise illumination at 395 nm of **6I** in *n*-heptane (blue spectrum in **b**) showing its photoconversion into **6H** (black spectrum in **b**) accompanied by the formation of I_2 (orange spectrum, magnified as inset in **b**). **c**: Scaled absorption (ε(385 nm, ACN) = 6638 $M^{-1}\,cm^{-1}$; ε(387 nm, *n*-heptane) = 8240 $M^{-1}\,cm^{-1}$) and emission spectra of **6H** in degassed (solid curves) and non-degassed (dashed curves) acetonitrile. The emission was recorded while exciting at 300 nm. To note, the upscaled dark red spectrum shows only the phosphorescence contribution after subtraction of the pure fluorescence contribution. The grey dashed vertical lines indicate the estimated S_1 (crossing point of the normalized absorption and fluorescence spectra) and T_1 (inflection point of the blue edge of the phosphorescence spectrum) energies. **d**: Corresponding phosphorescence decays as indicated. The red curves show the mono-exponential fits. To note, in contrast to the transient absorption recordings in the ns to µs time range (Figure 3 and Figure S5), in transient emission recordings only a very low concentration of excited species ($<$150 nM, i.e., $<$1% of 15 µM) is generated so that a mono-exponential decay of the phosphorescence without any bimolecular reaction either between two excited-state species or one excited state and one ground state (vide infra) is observed (A typical diffusion-controlled bimolecular reaction with 15 µM ground state molecules in acetonitrile with a typical bimolecular rate of $2\cdot10^{10}\ M^{-1}\,s^{-1}$ would yield non-exponential kinetics with a lifetime in the order of 3 to 4 µs).

Materials and Methods

Samples

Racemic thio-helicene **6I** with an iodine at the 6-position of the naphthalene, as confirmed by the appearance of a singlet resonance signal at 8.44 ppm from the proton in 7-position in the ^{1}H-NMR spectrum (see Figure S1a), was a kind gift from Dr. Parham (Merck) and its synthesis is described in Ref. [44]. The racemic compound **6H** was obtained through photoconversion from **6I** in *n*-heptane (20 mg in 20 mL) by irradiation with UV light (LED with an emission maximum at 365 nm, CUN66A1B, Seoul Viosys) for 15 h. The formed molecular iodine was subsequently washed off in repeated steps of shaking the irradiated solution with an aqueous sodium thiosulfate solution ($c\approx1$ M), by which the iodine was reduced to iodide and the iodide was then transferred to the aqueous phase. After separation of the aqueous phase the *n*-heptane was removed by evaporation in the vacuum. For recording data under molecular oxygen free conditions, the samples were degassed by cycles of freeze, pump thaw at a vacuum in the order of 10^{-6} mbar.

Stationary Spectroscopy

Electronic absorption and emission spectra in the UV/Vis were recorded at room temperature with a referenced single beam UV-1800 spectrometer (Shimadzu) and with a Fluorolog 3-22 system (Horiba Jobin Yvon), respectively. The emission quantum yields were determined with a C9920-02 system equipped with a Spectralon® integration sphere (Hamamatsu Photonics). For step-wise illumination and recording of absorption spectra the sample (2 mL) in a 10 mm (probing) x 10 mm (excitation) cuvette was placed in a self-constructed cuvette holder for illumination inside the absorption spectrometer orthogonally to the detection beam and for continuously stirring of the sample during the illumination periods. The sample was illuminated for 10 min steps in between the absorption spectrum recordings with UV light (LED with an emission maximum at 395 nm).

Nanosecond-Transient Emission

Emission decay curves were measured with the time correlated single photon counting technique (TCSPC) using the Fluorolog in combination with a P7887 counter (FAST ComTec, resolution 250 ps). The sample was excited at 378 nm with a diode laser (Δt ≈100 ps, Horiba picobrite PB-375L).

Femtosecond-Transient Absorption

The time-resolved absorption in the UV/Vis spectral range on the fs to ns time range was recorded with an in-house built setup as described previously.[45,46] The corresponding sample in acetonitrile located in a quartz cell with 1 mm pathlength was excited at $\lambda_{exc}=$ 310 nm, with a pulse energy of *ca.* 300 nJ and co-linearly probed with a white-light supercontinuum (WLSC, focussing 800 nm pulse of *ca.* 1 mJ into a 5 mm thick CaF_2 disc). The spot sizes for the pump and probe pulses at the sample position were *ca.* 80 μm and *ca.* 40 μm, respectively. The sample was stirred by a magnetic stirrer bar rotating in the plane of the quartz cell driven by a rotating magnet. The time axis was chosen to be linear from −1 ps up to 2.0 ps in 20 fs steps and logarithmic afterwards, until the end of the delay stage corresponding to 6.5 ns. 200 transient absorption spectra were recorded at each delay position of a single scan. Prior to averaging each single spectrum was corrected for the dark current on the camera and for the fluctuations in the probe spectrum by referencing *via* a second camera. Averaging of 10 independent scans resulted in the final spectra. For recording the pure population dynamics of all excited states, the polarization between pump and probe pulses was set to magic angle (54.7°)[47,48] via a λ/2 plate in the pump beam path. The averaged pre-t_0 laser scatter signal was subtracted from the data and the *ca.* 2 ps chirp of the WLSC is corrected for prior to data analysis using the coherent artefact as an indicator for time zero at each wavelength.[49,50] Further analysis of the data was performed without any smoothing or filtering procedures applied to the data.

Microsecond-Transient Absorption

Transient absorption in the time ranges up to 100 μs was measured with a setup using a combination of a spectrograph and a streak camera for detection. The sample was either stirred or pumped through in a rectangular cuvette with 10 mm×10 mm or 10 mm×2 mm cross section, respectively. It was excited on the long side with the third harmonic ($\lambda_{exc}=355$ nm) of a Nd:YAG laser (Surelite II, Continuum, $\Delta t\approx10$ ns) through a cylindrical lens. The probe beam from a pulsed Xe lamp (150 W, 03-102 arc lamp pulser, Applied Photophysics, *ca.* 2 ms pulse duration) was guided by toroidal mirrors (aluminium-coated blanks of eyeglass lenses, Rodenstock) through the sample perpendicular to the excitation and imaged onto the entrance slit of a spectrograph (Bruker 200is). The dispersed light was analyzed with a streak camera (C7700 Hamamatsu Photonics) und the streak image recorded by a CCD camera (ORCA-CR, Hamamatsu Photonics). A typical measurement is the average of 100 excitation cycles, each producing 4 streak images ('laser and probe', 'dark', 'probe only', and 'dark'). The performance of the streak camera system has been described in detail in Refs. [51, 52].

Quantum Chemical Calculations

Electronic structure calculations using the DFT method were done with the ORCA programs,[53,54] employing the B3LYP/G functional and the def2-SVP basis set. The geometries of the states S_0, S_1, T_1, T_2, and T_3 were optimized, and their hessian matrices calculated. These serve as input for the ESD (excited state dynamics) module of ORCA which calculates spin-orbit coupling matrix elements (SOCME) and their derivatives with respect to the normal coordinates (see Table S1 for the SOCME and Supporting ZIP file containing the derivatives of these SOCME with respect to all normal coordinates of the final state). ISC rate constants were calculated with a home-written program which reads the geometries and hessians of the initial and final states, the SOCME and their derivatives. The formulas presented by Baiardi *et al.*[55] and de Souza *et al.*[56,57] for fluorescence emission rates were implemented. These are easily modified for ISC rates by replacing the three components of the dipole operator by the spin-orbit coupling operator for the three triplet sublevels. Both sets of formulas are almost equivalent and delivered identical results.

Relaxed surface scans were performed along the distance between carbon 1 and carbon 14 from $R(C_1–C_{14})=1.45$ Å (closed form) to $R(C_1–C_{14})=3.05$ Å (minimum of the open form). Since all attempts using the ORCA programs failed, the Firefly QC package (formerly PC-GAMESS),[58] which is partially based on the GAMESS(US)[59] source code, was used employing a CASSCF(10|10) wavefunction and the def2-SVP basis set. Firefly is able to strictly keep the point group symmetry and a particular irreducible representation for the wavefunction.

Results and Discussion

Photoconversion, Excited Singlet and Triplet State Energies, and Emission Properties

The absorption spectrum of **6I** (blue line in Figure 1b) shows a first absorption band rich of vibrational structure with an origin at 388 nm (25770 cm^{-1}, 3.20 eV). During irradiation with light of a 395 nm LED the spectrum is converted to that of **6H** (black line in Figure 1b), which is confirmed by NMR spectroscopy after isolation of the product (see Figure S1). The sequence of absorption spectra after stepwise illumination for 10 minutes reveals several clear isosbestic points (see Figure 1b), indicating a clean photoconversion without further photodecomposition of **6H**. Further, a weak and broad band with maximum at

Research Article
doi.org/10.1002/cptc.202300343

510 nm appeared parallel with **6H** formation, which is assigned to molecular iodine I_2 (see Figure 1b and Figure S2).[50]

Apparently, excitation of **6I** into the $S_1 \leftarrow S_0$ absorption band leads to homolytic cleavage of the iodine atom at C_6 with high quantum yield.[60–63] The resulting radicals in solution are stabilized by hydrogen abstraction from the solvent, while the iodine atoms combine to molecular iodine.

6H shows weak fluorescence ($\Phi_{fl} \approx 1\,\%$) and phosphorescence ($\Phi_{ph} \approx 0.5\,\%$) peaking at *ca.* 381 and 560 nm, respectively (see Figure 1c). The phosphorescence spectrum is obtained as the difference of the emission spectra from an air-saturated sample and a degassed sample. Fluorescence and absorption show mirror symmetry with a very small Stokes shift (*ca.* 1000 cm^{-1}). The S_0 to S_1 energy gap is estimated from the crossing point of the normalized absorption and fluorescence spectra to 3.26 eV (26300 cm^{-1}, Figure 1c). The inflection point of the rising edge of the phosphorescence spectrum at 515 nm provides an estimate for the S_0 to T_1 energy of 2.41 eV (19450 cm^{-1}, Figure 1c). The triplet of **6H** decays with a rate constant of $1.4 \cdot 10^3\ s^{-1}$ ($\tau = 700\ \mu s$), whereas the triplet of **6I** decays much faster with a rate constant of $2.1 \cdot 10^4\ s^{-1}$ ($\tau = 48\ \mu s$) in accordance with the expected internal heavy atom effect of iodine.

Excited State Dynamics Including Triplet State Formation

Following excitation at 310 nm, excited-state absorption (ESA) accompanied by ground-state bleach (GSB) is observed for **6H** and **6I** as evidenced by a very broad positive absorption spectrum covering the entire experimental UV/Vis spectral range intersected by the negative or partially reduced positive absorption features of the corresponding ground-state spectrum and the stimulated emission (SE) spectrum (Figure 2a, d). For both molecules, the initially formed ESA is similar and shows small spectral shifts on a sub-ps and a 10 to 20 ps timescale until the overall spectral shape settles. Two exponentials are required in a global fit on these data of the initial

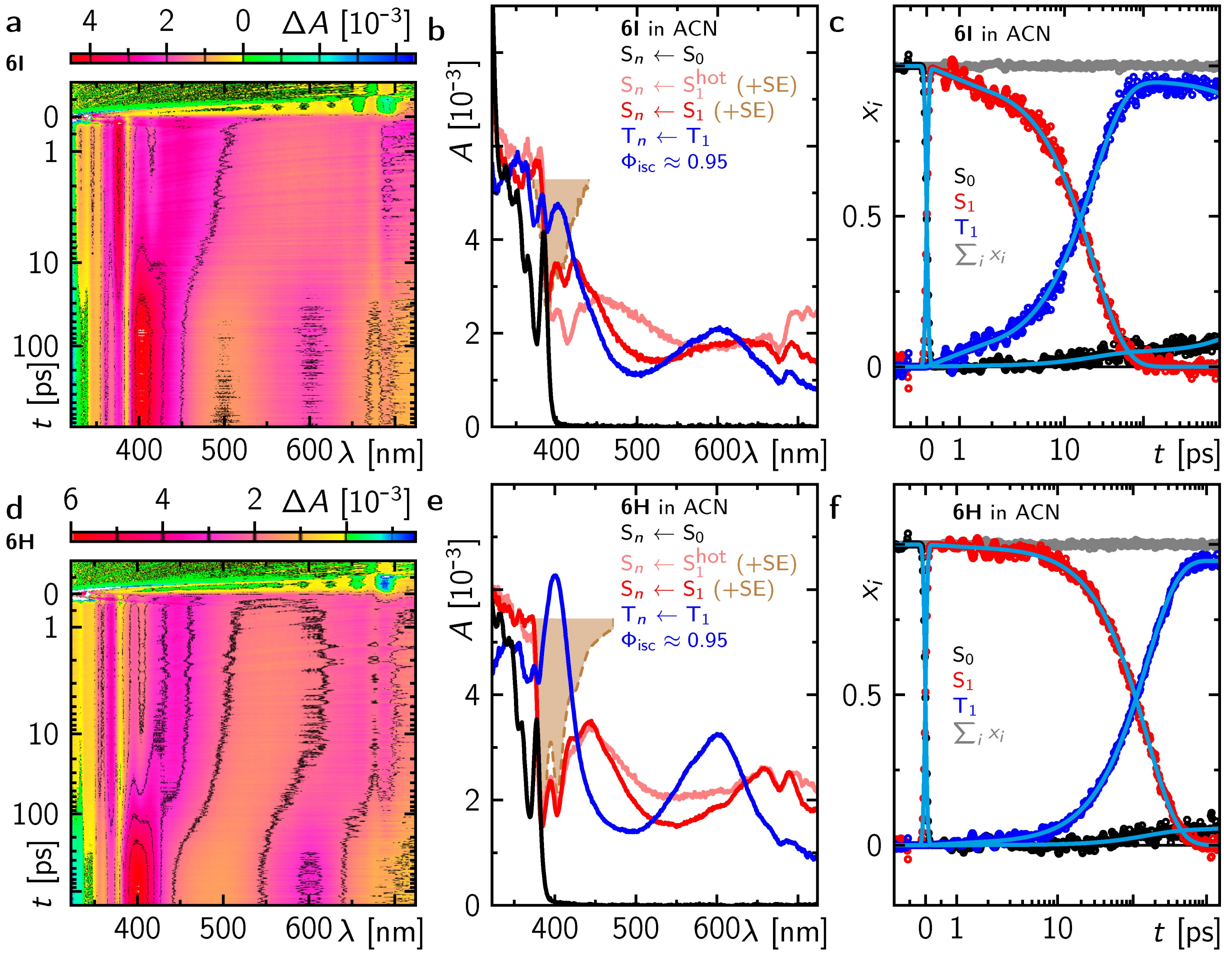

Figure 2. Transient absorption data on fs to ns time scale in the UV/Vis spectral range of **6H** (**a**–**c**) and **6I** (**d**–**f**) in acetonitrile following excitation at $\lambda_{exc} = 310$ nm recorded under magic angle conditions. **a**, **d**: Temporally and spectrally resolved transient absorption data matrices. **b**, **e**: Species-associated spectra contributing to the data in **a** and **b** as indicated. To note, the spectrum of the hot S_1 (light red) is obtained after addition of the two decay-associated difference spectra with the two shortest lifetimes (showing only small amplitudes that resemble the first derivative of the main transient contributions), that approximate the dynamics of small spectral shifts arising from intramolecular vibrational energy redistribution (IVR) and intermolecular vibronic energy transfer (IET) to the environment, to the settled/equilibrated S_1 spectrum (red). **c**, **f**: Corresponding concentration time profiles (x_i) in the same color coding as in **b** and **e**. The cyan lines correspond to the global fit and the grey points represent the sum of all x_i. SE: stimulated emission contribution (brown dashed curves, $F(\lambda)_{stim} \propto F(\lambda)_{spon}\, \lambda^4$;[65]).

Research Article
doi.org/10.1002/cptc.202300343

dynamics up to 50 ps to provide a good description. The resulting decay-associated difference spectra (DADS) with lifetimes of *ca.* 500 fs and *ca.* 15 ps in both cases show either only small amplitudes or are spectrally slightly shifted to the main transient contributions, which indicates their spectral shifting on these time scales (Figure S3). Thus, these fast spectral dynamics can be assigned to intramolecular vibrational energy redistribution (IVR) and intermolecular vibronic energy transfer (IET) to the environment until the thermally equilibrated first excited singlet state is formed (compare light red and red spectra in Figure 2b, e). With longer delay, the overall spectral shape of the transient absorption changes significantly as evidenced by the formation of two new positive absorption features peaking at *ca.* 400 and 600 nm in both cases. However, the timescale is significantly different for **6H** and **6I**. A single exponential covers these spectral changes (Figure S3) and the lifetimes are 150 ps and 20 ps for **6H** and **6I**, respectively. Until the experimental time window of *ca.* 6 ns the newly formed spectrum does not decay, and no further spectral signatures are observed, so that in the global fit on the entire data set in each case a further fourth exponential with a lifetime $\gg$ 6 ns is required (Figure S3). Thus, when considering only the dynamics starting from the equilibrated S_1 state, a model that includes only S_1 decay either into the ground state or the triplet state and a subsequent triplet decay into the ground state, that is not resolved in these data, is sufficient to determine the yield and simultaneously the rate of intersystem crossing. The mathematical formulation and the relationship between DADS and species associated spectra (SAS) for this model has been presented for instance in[45,64] giving the following equations for determining the S_1 (S_{S_1}) and the T_1 (S_{T_1}) absorption spectrum from the two relevant DADS (D_i with corresponding fitted rate constants κ_i) and the ground state spectrum (S_{S_0})

$$S_{S_1} = \frac{(D_1 + D_2)}{c_0} + S_{S_0}$$

$$S_{T_1} = \frac{(\kappa_1 - \kappa_2)D_2}{c_0 \Phi_{ISC} \kappa_1} + S_{S_0}$$

where c_0 is the fraction of molecules initially excited from the ground state and Φ_{ISC} is the triplet yield. Subsequent variation of first c_0 and then Φ_{ISC} (see Figure S3) results in physically reasonable SAS that are positive and do not show any of the characteristic bands – in particular the sharp ground state features – of the respective other species (Figure 2b, e). Inverting the original data matrix with these SAS yields these concentration time profiles including the noise from the experiment, which sum up to 1 providing further evidence for an appropriate scaling of the SAS (Figure 2c, f). The spectrum of the hot S_1 (light red curve in Figure 2b, e) is obtained by addition of the two decay-associated difference spectra with the two shortest lifetimes ascribing for the fast dynamics on the first 50 ps. To note, in the case of the S_1 spectra also significant contribution of the SE is visible in the spectra (brown curves in Figure 2b, e). Based on this model both molecules have an intersystem crossing quantum yield of *ca.* 90 % with corresponding rates k_{ISC} of $6 \cdot 10^9\ s^{-1}$ ($\tau = 166$ ps) and $4.5 \cdot 10^{10}\ s^{-1}$ ($\tau = 22$ ps) for **6H** and **6I**, respectively.

Light-Induced Transient Ring Closure Reaction

The triplet state dynamics of **6H** in degassed acetonitrile after excitation at 355 nm on a 100 μs temporal range are shown in Figure 3a. Since the S_1 state decay is much faster than the time resolution of the performed experiment, the only species expected are the T_1 state and the ground state S_0. However, a further rate constant is required for a reasonable fit yielding a DADS with significantly different spectra contributions (see Figure S4). Thus, a further intermediate must be postulated. The kinetic scheme adopted for the analysis assumes that the T_1 state decays either to this intermediate or to the ground state, and the intermediate subsequently decays to the ground state on a slower time scale. The SAS in Figure 3b suggest that the proposed intermediate has a spectrum similar to the T_1 state with an additional absorption band/shoulder at *ca.* 450 nm and small deviations between *ca.* 325 and 400 nm. Since the transient emission of the phosphorescence under conditions of

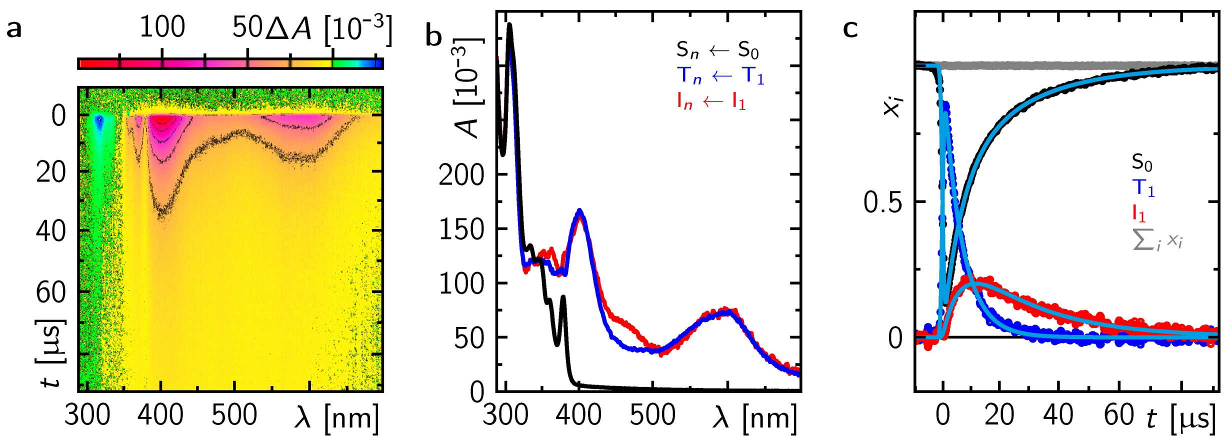

Figure 3. Transient absorption data of **6H** in degassed acetonitrile in the 100 μs temporal range and UV/Vis spectral range after excitation at 355 nm ($E_{exc} = 12.2$ mJ). **a**: Temporally and spectrally resolved transient absorption data matrices. **b**: Species associated spectra contributing to the data in **a** as indicated. **c**: Corresponding concentration time profiles in the same color coding as in **b**. The cyan lines correspond to the global fit.

doi.org/10.1002/cptc.202300343

very low concentration of excited species is mono-exponential, thus, showing the intrinsic T_1 decay into the ground state (Figure 1d), the significantly faster T_1 decay and simultaneous rise of a transient species under conditions of much higher concentration of excited species (ca. 14.8 μM, i.e., 32% of 45 μM) demonstrates a bimolecular reaction between two excited triplet states. This is further confirmed by an excitation energy dependence of the T_1 decay and the intermediate formation (Figure S5). A triplet-triplet annihilation forming S_1 and S_0 is excluded, since – apart from the fact that the S_1 decay would be faster than its formation – the spectrum of the intermediate does not resemble spectral absorption features of the S_1 (compare Figure 2e). Due to the high similarity between the T_1 spectrum and the spectrum of the intermediate also an electron transfer between two T_1 species seems to be unlikely, as the putative radical anion and cation were expected to show very different absorption spectra compared to the T_1 spectrum (Figure S6). Thus, a possible candidate for such an intermediate is the species generated by ring closure of the ends of the helicene system along the carbon 1 and carbon 14 bond, which is mediated by complex formation between two excited triplet species (see Figure 5, *vide infra*).

Theoretical Considerations of Spin Orbit Coupling and the Ring Closure Reaction

The energies of the states S_0, S_1, T_1, T_2, and T_3 at each of the optimized geometries for the parent helicene, oxohelicene, and thiohelicene (**6H**) are shown in Table 1. The reference energy in each case is the optimized S_0 state. The diagonal elements in each matrix correspond to the adiabatic energy gaps that are relevant for the ESD calculations. For the states S_0 and S_1 this should correspond to the origin transition of absorption and fluorescence.

Energy differences in each column correspond to vertical excitation energies, *i.e.*, band maxima in experimental spectra. A comparison of calculated and available experimental energy values for the electronic origin transitions in Table 2 shows very good agreement for the experimental data from fluorescence and phosphorescence spectra. Thus, a similar accuracy also for other states of these systems may be assumed.

According to the TD-DFT calculations, the first three triplet states have an energy below the energy of the first excited singlet. Hence, ISC from S_1 to these three triplet states is considered. The ISC rate constants calculated as a function of the energy gap between S_1 and the final triplet state are displayed in Figure 4.

For all three final triplet states, the rates increase in the sequence helicene $<$ oxohelicene $<$ thiohelicene (**6H**). The rate constants at these energies are summarized in Table 3.

Table 1. Energies (in cm^{-1}) of the states S_0, S_1, T_1, T_2, and T_3 at their optimized geometries, relative to the energy of the optimized S_0 ground state of helicene, oxohelicene, and thiohelicene (**6H**).

helicene			**Geometry**		
state	**S_0**	**S_1**	**T_1**	**T_2**	**T_3**
S_0	0	930	2056	1022	937
S_1	26115	25164	26482	25698	25253
T_1	20712	19968	19241	20299	20257
T_2	23271	22663	23863	22195	22765
T_3	24182	23244	25357	23812	23089
oxohelicene			**Geometry**		
state	**S_0**	**S_1**	**T_1**	**T_2**	**T_3**
S_0	0	1250	2062	1234	797
S_1	30492	29250	29476	29784	29918
T_1	21996	20103	19853	20911	21065
T_2	26668	25979	26466	25416	26671
T_3	27633	27525	27986	28147	26818
Thiohelicene (6H)			**Geometry**		
state	**S_0**	**S_1**	**T_1**	**T_2**	**T_3**
S_0	0	716	2084	686	1332
S_1	28061	27359	28119	27457	28250
T_1	21348	20249	19226	20365	20103
T_2	24334	23692	24672	23600	24769
T_3	26306	25959	25869	26134	24962

Table 2. Comparison of the theoretical values with available experimental data for helicene, oxohelicene, and thiohelicene (**6H**).

compound	helicene		oxohelicene		thiohelicene	
	exp.	theo.	exp.	theo.	exp.	theo.
S_0–S_1 gap/cm^{-1}	24550[66] 24390[11] 24500[67]	25164	28570[68]	29250	26600[44] 26280[69]	27359
S_0–T_1 gap/cm^{-1}	19550[66] 19050[11] 19400[67]	19241		19853	19400[69]	19226
Φ_{fl}/%	4[11]		20[68]		1[69]	
Φ_{isc}/%	91[11]				$>$67[69]	
$\tau(S_1)$/ns	14.5		5.1			
***k*(ISC)/10^6 s^{-1}**	62.8 a)		157 a)		5900[69]	

a) Calculated from singlet decay time and triplet yield.

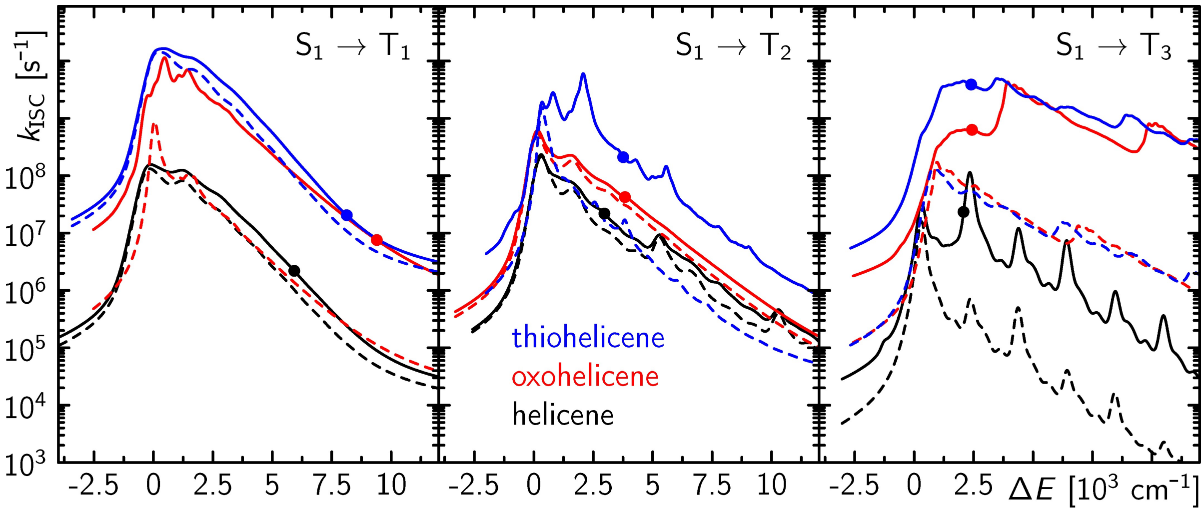

Figure 4. Calculated ISC rate constants as function of the adiabatic S_1–T_n energy gap for helicene (blue), oxohelicene (red), and thiohelicene (**6H**, black). Dotted curves indicate the Franck-Condon contribution, full lines the total rate constant including the Herzberg-Teller contributions.

Table 3. Adiabatic energy gaps and ISC rate constants from TD-DFT and ESD calculations for helicene, oxohelicene, and thiohelicene (**6H**).

	helicene		oxohelicene		thiohelicene (6H)	
	ΔE/cm^{-1}	k/10^6 s^{-1}	ΔE/cm^{-1}	k/10^6 s^{-1}	ΔE/cm^{-1}	k/10^6 s^{-1}
S_1–T_1	5923	2.20	9397	7.58	8133	20.52
S_1–T_2	2969	21.96	3836	42.45	3758	210.9
S_1–T_3	2075	23.45	2432	632.3	2397	3896.0
sum (1–2)		24.16		50.03		231.4
sum (1–3)		**47.61**		**682.3**		**4127**
exp.		62.8		157		5900

Experimental values for the ISC rate constants can be estimated from the fluorescence decay rate and the triplet yield. For oxohelicene the triplet yield was not reported but an upper limit of 80% can be estimated from the fluorescence yield (20%).

To note, the experimental rate constant increases from helicene to oxohelicene by a factor of 2.5, and to thiohelicene (**6H**) by a factor of 94. In each case, the experimental rate is more than one or two orders of magnitude larger than the value calculated for the S_1–T_1 ISC. Apparently, the ISC to a higher triplet state is dominant. Considering also the S_1–T_2 channel, this results in rate constants that are still too low by a factor of 2.6 for helicene and by a factor of 25 for thiohelicene (**6H**). Further addition of the S_1–T_3 channel results in rather good agreement for helicene (calc.: $4.8 \cdot 10^7$ s^{-1}, exp.: $6.3 \cdot 10^7$ s^{-1}) and thiohelicene (**6H**, calc.: $4.1 \cdot 10^9$ s^{-1}, exp.: $5.9 \cdot 10^9$ s^{-1}). Hence, the calculated values are *ca.* 20% smaller than the experimental ones. However, for oxohelicene the calculated rate overestimates the experimental value by more than a factor of 4.

Given the large number of calculated parameters that enter the ESD formulas, together with the assumption of a harmonic potential energy surface for all states, a deviation of less than a factor of 2 can be considered as a very good agreement between calculation and experiment. We conclude that the channel S_1–T_3 represents the dominant contribution for ISC in the molecule thiohelicene (**6H**) and probably also in helicene. The discrepancy in the case of oxohelicene might indicate that ISC from S_1 to T_3 is energetically not accessible in this compound.

In an estimated approach to elaborate the contribution of the helicity to the SOC, the SOCME were also calculated for the planar reference molecules hexacene, oxohexacene, and thiohexacene (Figure S7 and Table S3), that are composed of the same sequence of rings, albeit with different connectivity. As expectable, all SOCME between S_1 and the $M = \pm 1$ substates of the T_1 and T_2 states are forbidden for all three reference compounds. Oxygen or sulfur induces a minute value of the SOC for the $M = 0$ transition, which is, however, negligible compared to the helical compounds. Thus, one can conclude that the helical arrangement has some effect, e.g., inducing a value of 0.49 cm^{-1} for S_1–T_1 of helicene. In the planar compound, sulfur induces a value of 0.0035 cm^{-1}, which one may consider as the "pure" heavy atom effect. However, in the helical sulfur compound, the SOCME increases to 4.99 cm^{-1}. Obviously, there is a non-trivial cooperation between the helical arrangement and the heavy atom effect.

The ring closure reaction of **6H** along C_1 and C_{14} distance was investigated by performing relaxed surface scans (symmetry restricted to point group C_2) for the singlet ground state of ^1A symmetry and the two lowest triplet states of ^3A and ^3B symmetries (Figure 5). The two triplet paths cross near $R(C_1–C_{14}) = 2.2$ Å The ^3A state is lowest for the open form and the ^3B state is T_1 at the ring closed form. At this closed configuration ^3B and ^1A are quasi degenerate with an energy splitting of only 150 cm^{-1}, *i.e.*, the ring closed form is a biradical without any charge transfer character (see Figure 5) – in agreement with the fact that no valid neutral Lewis structure can be drawn for this geometry. Further, this explains why the single reference DFT approach is not able to treat this problem properly: The reference state is not closed shell, and the conical intersection between the two triplet states inhibits convergence. The crossing between the two triplet states occurs *ca.* 20 kcal/mol above the minimum of the ^3A state, which should be the primarily populated triplet state after excitation of the open form (*vide supra).* Accordingly, a reaction to the ring closed form should be possible on a microsecond time scale in a bimolecular complex formation (vide supra). The minimum of ^3B is at about the same energy as that of the ^3A, *i.e.*, equilibrium between both forms is possible if the ISC from ^3B to the ^1A biradical is slow. Therefore, it is proposed that the second

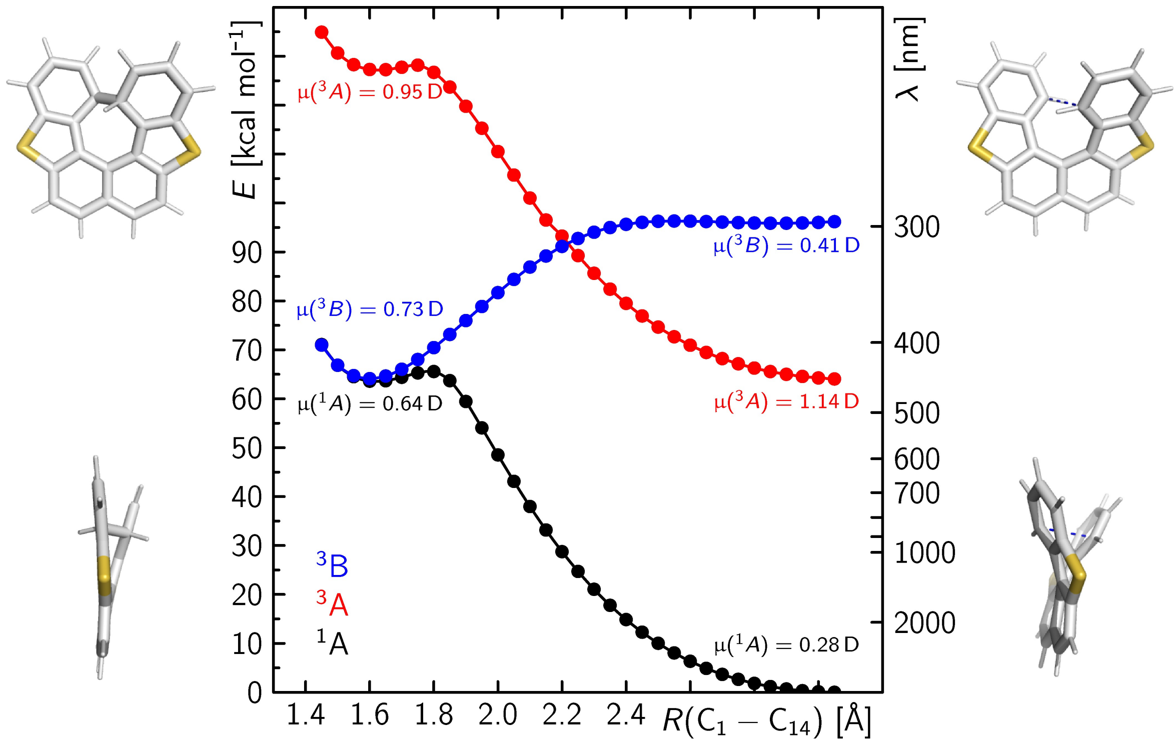

Figure 5. Calculated potential surfaces of **6H** along the carbon 1 to carbon 14 distance (solid or blue dashed bond in the structures on the left and right, respectively) for the singlet ground state (^1A) and the two lowest triplet states (^3A and ^3B) based on CASSCF(10|10)//def2-SVP level of theory. To note, for each potential shown the corresponding state was structurally optimized so that the geometries between the states differ for each distance $R(C_1–C_{14})$. The dipole moments of the six structures at the local minima are also given in the corresponding color. Color code of the stick representation: hydrogen – white; carbon – grey; sulfur – yellow.

Chemistry Europe
European Chemical Societies Publishing

intermediate observed on the microsecond time scale can be assigned to the biradical $^3B/^1A$ species.

Conclusions

Following excitation by UV light, the thiohelicene **6H** undergoes efficient ($\Phi_{isc} \approx 90\%$) ISC to the triplet state. This triplet state shows a rather long lifetime (700 µs in degassed ACN) and emits detectable phosphorescence (peak 560 nm) at room temperature. Transient absorption experiments indicate an intermediate en route from T_1 back to S_0, which is assigned to a biradical formed by ring closure of the two benzene units at the ends of the helix. The compound appears to be rather photostable, in contrast to its iodine derivative **6I** which decomposes quickly yielding **6H** and molecular iodine.

Comparison of quantum-chemical calculations with available experimental data for the corresponding oxo-helicene and parent helicene indicate that helical distortion and the heavy atom effect cooperate in the high efficiency of ISC for **6H**. We propose that in search of efficient triplet sensitizers, small deviations from planarity should be employed to enable SOC, but further boost ISC by using third row elements as "mild" heavy atoms that do not compromise photochemical stability.

Acknowledgements

We thank Dr. Parham from Merck KGaA (Darmstadt) for kindly providing the racemic thiohelicene with an iodine at 6-position **6I** and Prof. Burkhard König for fruitful discussions. Financial support by the Deutsche Forschungsgemeinschaft (DFG, German Research Foundation) within TRR 325 – 444632635 (project A5) is gratefully acknowledged. Open Access funding enabled and organized by Projekt DEAL.

Conflict of Interests

The authors declare no conflict of interest.

Data Availability Statement

The data that support the findings of this study are available from the corresponding author upon reasonable request.

[1] N. A. Romero, D. A. Nicewicz, *Chem. Rev.* **2016**, *116*, 10075.
[2] J. Großkopf, T. Kratz, T. Rigotti, T. Bach, *Chem. Rev.* **2021**, *122*, 1626.
[3] A. Kamkaew, S. H. Lim, H. B. Lee, L. V. Kiew, L. Y. Chung, K. Burgess, *Chem. Soc. Rev.* **2012**, *42*, 77.
[4] J. Zhao, W. Wu, J. Sun, S. Guo, *Chem. Soc. Rev.* **2013**, *42*, 5323.
[5] M. Lan, S. Zhao, W. Liu, C.-S. Lee, W. Zhang, P. Wang, *Adv. Healthcare Mater.* **2019**, *8*, 1900132.
[6] G. J. Hedley, A. Ruseckas, I. D. W. Samuel, *Chem. Rev.* **2017**, *117*, 796.
[7] G. Zhang, J. Zhao, P. C. Y. Chow, K. Jiang, J. Zhang, Z. Zhu, J. Zhang, F. Huang, H. Yan, *Chem. Rev.* **2018**, *118*, 3447.
[8] M. A. El-Sayed, *J. Chem. Phys.* **1963**, *38*, 2834.
[9] M. Baba, *J. Phys. Chem. A* **2011**, *115*, 9514.
[10] O. E. Weigang Jr., J. A. Turner, P. A. Trouard, *J. Chem. Phys.* **1966**, *45*, 1126.
[11] M. Sapir, E. V. Donckt, *Chem. Phys. Lett.* **1975**, *36*, 108.
[12] N. I. Nijegorodov, W. S. Downey, *J. Phys. Chem.* **1994**, *98*, 5639.
[13] D. Beljonne, Z. Shuai, G. Pourtois, J. L. Bredas, *J. Phys. Chem. A* **2001**, *105*, 3899.
[14] D. Huertas-Hernando, F. Guinea, A. Brataas, *Phys. Rev. B* **2006**, *74*, 155426.
[15] K. Schmidt, et al., *J. Phys. Chem. A* **2007**, *111*, 10490.
[16] K. Nagarajan, A. R. Mallia, K. Muraleedharan, M. Hariharan, *Chem. Sci.* **2017**, *8*, 1776.
[17] Z. Wang, L. Huang, Y. Yan, A. M. El-Zohry, A. Toffoletti, J. Zhao, A. Barbon, B. Dick, O. F. Mohammed, G. Han, *Angew. Chem. Int. Ed.* **2020**, *59*, 16114.
[18] Y. Dong, B. Dick, J. Zhao, *Org. Lett.* **2020**, *22*, 5535.
[19] X. Zhang, Z. Wang, Y. Hou, Y. Yan, J. Zhao, B. Dick, *J. Mater. Chem. C* **2021**, *9*, 11944.
[20] J. Heitmüller, R. Fröhlich, R. Renner, F. Würthner, T. Brixner, *Phys. Chem. Chem. Phys.* **2023**, *25*, 17214.
[21] M. Koli, S. Gupta, S. Chakraborty, A. Ghosh, R. Ghosh, A. P. Wadawale, T. K. Ghanty, B. S. Patro, S. Mula, *Chem. Eur. J.* **2023**, *29*, e202301605.
[22] F. Kuemmeth, S. Ilani, D. C. Ralph, P. L. McEuen, *Nature* **2008**,*452*, 7186.
[23] G. A. Steele, F. Pei, E. A. Laird, J. M. Jol, H. B. Meerwaldt, L. P. Kouwenhoven, *Nat. Commun.* **2013**, *4*, 1.
[24] J.-S. Jeong, H.-W. Lee, *Phys. Rev. B* **2009**, *80*, 075409.
[25] Y. Yan, et al., *J. Phys. Chem. B* **2021**, *125*, 6280.
[26] R. Ahmed, A. K. Manna, *J. Phys. Chem. A* **2022**, *126*, 6594.
[27] X. Zhang, A. A. Sukhanov, X. Liu, M. Taddei, J. Zhao, A. Harriman, V. K. Voronkova, Y. Wan, B. Dick, M. D. Donato, *Chem. Sci.* **2023**, *14*, 5014.
[28] M. Imran, H. Cao, J. Zhao, G. Mazzone, *J. Phys. Chem. A* **2023**, *127*, 4856.
[29] J. C. Koziar, D. O. Cowan, *Acc. Chem. Res.* **1978**, *11*, 334.
[30] K. N. Solov'ev, E. A. Borisevich, *Phys.-Usp.* **2005**, *48*, 231.
[31] M. Gingras, *Chem. Soc. Rev.* **2013**, *42*, 968.
[32] M. Gingras, G. Félix, R. Peresutti, *Chem. Soc. Rev.* **2013**, *42*, 1007.
[33] M. Gingras, *Chem. Soc. Rev.* **2013**, *42*, 1051.
[34] J. Crassous, I. Stara, I. Stary, editors, *Helicenes - Synthesis, Properties and Applications*, 1st ed. (Wiley-VCH, Weinheim, **2022**).
[35] H. Zhu, M. Li, J. Hu, X. Wang, J. Jie, Q. Guo, C. Chen, A. Xia, *Sci. Rep.* **2016**, *6*, 1.
[36] Y. Nakakuki, T. Hirose, H. Sotome, H. Miyasaka, K. Matsuda, *J. Am. Chem. Soc.* **2018**, *140*, 4317.
[37] Y. Nakakuki, T. Hirose, H. Sotome, M. Gao, D. Shimizu, R. Li, J. Hasegawa, H. Miyasaka, K. Matsuda, *Nat. Commun.* **2022**, *13*, 1.
[38] M. Morgenroth, M. Scholz, L. Guy, K. Oum, T. Lenzer, *Mol. Phys.* **2021**, *119*, e1959072.
[39] M. Morgenroth, M. Scholz, L. Guy, K. Oum, T. Lenzer, *Angew. Chem. Int. Ed.* **2022**, *61*, e202203075.
[40] D. Aranda, F. Santoro, *J. Chem. Theory Comput.* **2021**, *17*, 1691.
[41] Y. Liu, D. Aranda, F. Santoro, *Phys. Chem. Chem. Phys.* **2021**, *23*, 16551.
[42] V. M. Freixas, J. R. Rouxel, Y. Nam, S. Tretiak, N. Govind, S. Mukamel, *J. Am. Chem. Soc.* **2023**, *145*, 21012.
[43] H. Kudo, M. L. Tedjamulia, R. N. Castle, M. L. Lee, *J. Heterocycl. Chem.* **1984**, *21*, 185.
[44] J. Kaiser, A. Mekic, A. H. Parham, H. Buchholz, B. König, *Eur. J. Org. Chem.* **2020**, *2020*, 66.
[45] T. Pavlovska, D. Král Lesný, E. Svobodová, I. Hoskovcová, N. Archipowa, R. J. Kutta, R. Cibulka, *Chem. Eur. J.* **2022**, *28*, e202200768.
[46] J. Knorr, N. Sülzner, B. Geissler, C. Spies, A. Grandjean, R. J. Kutta, G. Jung, P. Nuernberger, *Photochem. Photobiol. Sci.* **2022**, *21*, 2179.
[47] H. E. Lessing, A. von Jena, *Chem. Phys. Lett.* **1976**, *42*, 213.
[48] S. Schott, A. Steinbacher, J. Buback, P. Nuernberger, T. Brixner, *J. Phys. B: At. Mol. Opt. Phys.* **2014**, *47*, 124014.
[49] U. Megerle, I. Pugliesi, C. Schriever, C. F. Sailer, E. Riedle, *Appl. Phys. B* **2009**, *96*, 215.
[50] S. Schott, L. Ress, J. Hrušák, P. Nuernberger, T. Brixner, *Phys. Chem. Chem. Phys.* **2016**, *18*, 33287.
[51] R.-J. Kutta, T. Langenbacher, U. Kensy, B. Dick, *Appl. Phys. B* **2013**, *111*, 203.
[52] B. Dick, U. Kensy, R. J. Kutta, *Phys. Sci. Rev.* **2019**, *4*, 20170179.
[53] F. Neese, *Wiley Interdiscip. Rev.: Comput. Mol. Sci.* **2012**, *2*, 1.
[54] F. Neese, *Wiley Interdiscip. Rev.: Comput. Mol. Sci.* **2018**, *8*, 1.
[55] A. Baiardi, J. Bloino, V. Barone, *J. Chem. Theory Comput.* **2013**, *9*, 4097.
[56] B. de Souza, F. Neese, R. Izsák, *J. Chem. Phys.* **2018**, *148*, 034104.
[57] B. de Souza, G. Farias, F. Neese, R. Izsák, *J. Chem. Theory Comput.* **2019**, *15*, 1896.

[58] *Firefly Home Page*, Alex A. Granovsky, Firefly version 8, www http://classic.chem.msu.su/gran/firefly/index.html.
[59] M. W. Schmidt, et al., *J. Comput. Chem.* **1993**, *14*, 1347.
[60] A. Levy, D. Meyerstein, M. Ottolenghi, *J. Phys. Chem.* **1971**, *75*, 3350.
[61] M. Kadi, J. Davidsson, A. N. Tarnovsky, M. Rasmusson, E. Åkesson, *Chem. Phys. Lett.* **2001**, *350*, 93.
[62] M. N. R. Ashfold, G. A. King, D. Murdock, M. G. D. Nix, T. A. A. Oliver, A. G. Sage, *Phys. Chem. Chem. Phys.* **2010**, *12*, 1218.
[63] S. K. Khani, B. Geissler, E. Engelage, P. Nuernberger, C. Hättig, *Phys. Chem. Chem. Phys.* **2021**, *23*, 7480.
[64] N. Archipowa, R. J. Kutta, D. J. Heyes, N. S. Scrutton, *Angew. Chem. Int. Ed.* **2018**, *57*, 2682.
[65] A. V. Deshpande, A. Beidoun, A. Penzkofer, G. Wagenblast, *Chem. Phys.* **1990**, *142*, 123.
[66] M. F. O'Dwyer, M. A. El-Bayoumi, S. J. Strickler, *J. Chem. Phys.* **2004**, *36*, 1395.
[67] W. Rhodes, M. F. Amr El-Sayed, *J. Mol. Spectrosc.* **1962**, *9*, 42.
[68] A. Mekic, *Entwicklung neuer blauer fluoreszenter Emitter für die Anwendung in organischen Leuchtdioden* (Doctoral thesis, University of Regensburg, Regensburg, **2019**).
[69] S. Bergwinkl, *Licht-induzierte Transferprozesse in Lösung* (Doctoral thesis, University of Regensburg, Regensburg, **2022**).

Manuscript received: December 21, 2023
Revised manuscript received: February 27, 2024
Accepted manuscript online: March 4, 2024
Version of record online: May 22, 2024